

# Flux closure during a substorm observed by Cluster, Double Star, IMAGE FUV, SuperDARN, and Greenland magnetometers

S. E. Milan<sup>1</sup>, J. A. Wild<sup>1,2</sup>, B. Hubert<sup>3</sup>, C. M. Carr<sup>4</sup>, E. A. Lucek<sup>4</sup>, J. M. Bosqued<sup>5</sup>, J. F. Watermann<sup>6</sup>, and J. A. Slavin<sup>7</sup>

<sup>1</sup>Department of Physics and Astronomy, University of Leicester, Leicester LE1 7RH, UK

<sup>2</sup>Department of Communication Systems, Lancaster University, Lancaster LA1 4WA, UK

<sup>3</sup>Laboratory of Planetary and Atmospheric Physics, University of Liege, Liege, B-4000 Belgium

<sup>4</sup>Department of Physics, Imperial College London, London SW7 2AZ, UK

<sup>5</sup>Centre d'Etude Spatiale des Rayonnements, CESR/CNRS, 31028 Toulouse Cedex, France

<sup>6</sup>Danish Meteorological Institute, Lyngbyvej 100, DK-2100 Copenhagen, Denmark

<sup>7</sup>Laboratory for Extraterrestrial Physics, NASA Goddard Space Flight Center, Greenbelt, Maryland, USA

Received: 30 June 2005 – Revised: 8 February 2006 – Accepted: 9 February 2006 – Published: 23 March 2006

**Abstract.** We examine magnetic flux closure during an extended substorm interval on 29 August 2004 involving a two-stage onset and subsequent re-intensifications. Cluster and Double Star provide observations of magnetotail dynamics, while the corresponding auroral evolution, convection response, and substorm current wedge development are monitored by IMAGE FUV, SuperDARN, and the Greenland magnetometer chain, respectively. The first stage of onset is associated with the reconnection of closed flux in the plasma sheet; this is accompanied by a short-lived auroral intensification, a modest substorm current wedge magnetic bay, but no significant ionospheric convection enhancement. The second stage follows the progression of reconnection to the open field lines of the lobes; accompanied by prolonged auroral bulge and westward-travelling surge development, enhanced magnetic bays and convection. We find that the tail dynamics are highly influenced by ongoing dayside creation of open flux, leading to flux pile-up in the near-tail and a step-wise down-tail motion of the tail reconnection site. In all, 5 dipolarizations are observed, each associated with the closure of  $\sim 0.1$  GWb of flux. Very simple calculations indicate that the X-line should progress down-tail at a speed of  $20 \text{ km s}^{-1}$ , or  $6 R_E$  between each dipolarization.

**Keywords.** Magnetospheric physics (Magnetotail; Solar wind-magnetosphere interactions; Storms and substorms)

## 1 Introduction

Substorms are a key component of the cycle of capture and release of the interplanetary magnetic field (IMF) by the terrestrial magnetosphere, now known as the Dungey cycle

*Correspondence to:* S. E. Milan  
(steve.milan@ion.le.ac.uk)

(Dungey, 1961), and the excitation of magnetospheric and ionospheric convection (e.g. Cowley and Lockwood, 1992; Lockwood and Cowley, 1992). Open magnetospheric field lines created by magnetic reconnection at the dayside magnetopause accumulate in the magnetotail lobes and must eventually be released by reconnection in the magnetotail neutral sheet. Current paradigms of substorm onset and evolution involve the development of a near-Earth neutral line (NENL) which must first reconnect already-closed magnetic flux of the plasma sheet before the open flux of the magnetotail lobes can be closed to complete the Dungey cycle (Hones et al., 1979). The pinched-off closed flux is observed as a plasmoid ejected down-tail once the reconnection reaches lobe field lines. Recent studies with Cluster suggest that plasmoid formation can occur within  $X = -19 R_E$ , placing the NENL (or multiple NENLs) somewhat closer to the Earth than previously thought (Slavin et al., 2003).

At present, the amount of flux that is closed during substorms, the duration of the delay from onset before the closure of open flux, and the rate of reconnection are uncertain. Based on a limited sample, Milan et al. (2005) suggested that each magnetotail lobe contained approximately 0.8 GWb of open flux prior to substorm onset, and that on average 0.2–0.5 GWb of flux are closed during each substorm, contributing to a magnetospheric flux throughput of  $3.5 \text{ GWb day}^{-1}$ , equivalent to an average cross polar cap potential drop of  $\sim 40 \text{ kV}$ . This capture and release of interplanetary magnetic field lines provides the momentum, energy and mass input necessary to drive all magnetospheric dynamics. The present paper examines in detail the flux transport during a three-hour substorm interval on 29 August 2004.

Recent studies (e.g. Slavin et al., 2002; Borälv et al., 2005) have shown that combined observations of magnetotail dynamics and ionospheric responses are necessary to achieve a fuller understanding of substorm phenomena. Especially if

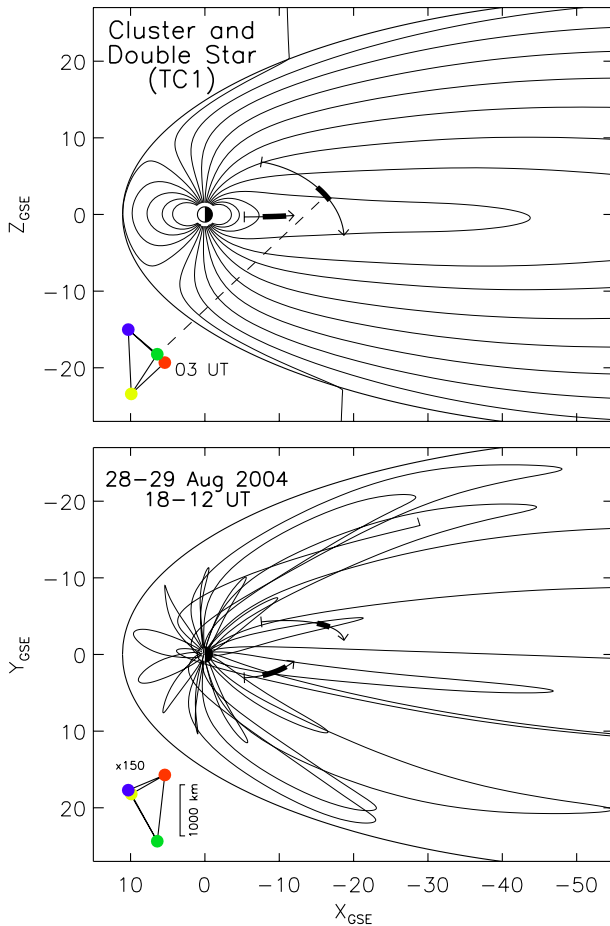


**Fig. 1.** GSE X-Z and X-Y cuts through the magnetosphere, showing field line traces through the T96 magnetic model. Shown also are the Cluster and Double Star trajectories for the intervals 18:00–12:00 UT, 28–29 August 2004, in the case of Cluster, and 00:00–06:00 UT, 29 August 2004, in the case of Double Star. In both cases, the highlighted portion of the trajectory indicates the interval 01:30 to 05:00 UT on 29 August, the period bracketing the substorm under consideration. In the bottom-left of each panel is the tetrahedral configuration of Cluster at 03:00 UT, blown up by a factor of 150.

changes in the open flux content of the magnetosphere are to be investigated, which cannot be determined from spacecraft in the tail, then global auroral morphology and/or convection measurements are required (e.g. Milan et al., 2003, 2006).

In this study, solar wind measurements are provided by the ACE spacecraft (McComas et al., 1988; Smith et al., 1988; Stone et al., 1988), located near the L1 point. Magnetotail observations are provided by the Cluster (Escoubet et al., 1997, 2001) and Double Star spacecraft missions, using the flux gate magnetometer (FGM, described by Balogh et al., 1997, 2001) and the Hot Ion Analyser (HIA) component of the Cluster Ion Spectrometry instrument (CIS, described by Rème et al., 1997, 2001). The ionospheric

currents associated with the development of the substorm current wedge are monitored by the Greenland magnetometer array (e.g. Popov et al., 2001). In conjunction, simultaneous views of the Northern Hemisphere convection pattern by the Super Dual Auroral Radar Network (SuperDARN, described by Greenwald et al., 1995), and the Southern Hemisphere auroral emissions by the Far-Ultraviolet Imager (FUV, described by Mende et al., 2000a, b) onboard the IMAGE spacecraft, allow the tail measurements to be placed within the context of the overall evolution of the substorm. We believe that an intensification of the auroral signature of the substorm  $\sim 20$  min after initial onset marks the transition from reconnection of closed flux to reconnection of open lobe flux, with the attendant release of plasmoids observed by Cluster.

## 2 Observations

In this section we provide a general overview of the interplanetary magnetic field measurements and corresponding magnetotail dynamics for an extended 12-h period, and subsequently focus in on detailed observations of the tail and ground observations of an isolated substorm.

### 2.1 Overview: IMF and Cluster

Figure 1 presents the orbital location of Cluster for the interval 18:00 UT, 28 August 2004, to 12:00 UT on the following day. The position of Double Star TC1 is also shown, for the period 00:00–06:00 UT, 29 August. Highlighted are the portions of the orbits between 01:30 to 05:00 UT, the duration of the substorm we investigate in detail. Cluster is located approximately  $16 R_E$  down-tail at this time,  $\sim 3 R_E$  above the equatorial plane, and slightly dawnwards of the noon-midnight meridian. Also at this time Double Star is passing outwards through geosynchronous orbit in the pre-midnight sector. Meanwhile, Geotail (not shown) provides measurements of the solar wind and interplanetary magnetic field (IMF) just upstream of the bow-shock. We find that both ACE and Geotail provide extremely similar observations, as long as a propagation delay of 60 min is applied to the ACE data, consistent with the solar wind velocity of  $350 \text{ km s}^{-1}$ . The GSM  $B_z$  component of the IMF, lagged now to the magnetopause, can be seen in the bottom panel of Fig. 2. Prior to 00:30 UT the IMF is mainly directed northwards; thereafter a southward turning marks the onset of a substorm growth phase, as will be discussed below. This growth phase is paused briefly by a short return to northwards IMF (01:00–01:15 UT), but after this time growth phase continues and expansion phase onset occurs near 01:50 UT. The IMF remains southwards after onset, eventually turning northwards again at 04:00 UT.

Panels (a–d) of Fig. 2 show the  $B_x$ ,  $B_y$ , and  $B_z$  components of the magnetic field, along with the total field

strength  $B_T$ , measured by FGM on Cluster 1 (C1) in the magnetotail; dashed red lines indicate Tsyanenko T96 (Tsyanenko and Stern, 1996) predictions of the field components. Also shown, in panels e and g, are the ion density and X-component of the ion velocity measured by HIA. Panel f shows the plasma  $\beta$ , the ratio of the plasma to the magnetic pressure, which helps distinguish between intervals when the spacecraft is located in the lobe, plasma sheet boundary layer (PSBL) or plasma sheet itself, in which (approximately)  $\beta < 0.1$ ,  $0.1 < \beta < 0.5$ , and  $\beta > 0.5$ , respectively. The plasma pressure, needed for the calculation of  $\beta$ , has been found from the HIA plasma density and temperature, in other words assuming that the pressure contribution from electrons is small.

Prior to 20:00 UT the magnetic field is dominated by a positive  $B_x$  component, consistent with the spacecraft being located in the northern lobe, though  $B_x$  and  $B_T$  are somewhat depressed below the T96 expectation. The observed ion densities of  $\sim 0.02 \text{ cm}^{-3}$  and  $\beta$  of  $\sim 10^{-3}$  are typical of the lobe.  $B_x$  and the total field strength fall with time as the spacecraft moves further from the Earth. At 20:45 UT there is a small increase in the  $B_z$  component of the magnetic field, indicative of a transition from a stretched tail-like field to a more dipolar field, a common signature of substorm onset (e.g. Heppner, 1967; Fairfield and Ness, 1970); this “dipolarization” is marked by a vertical dashed line. Approximately 30 min after this dipolarization the ion density increases to  $\sim 0.05 \text{ cm}^{-3}$  and  $\beta$  exceeds  $2 \times 10^{-2}$ , suggesting that the plasma sheet (or boundary layer) has expanded northward over the spacecraft in response to the substorm onset.

After the southward turning of the IMF at 00:40 UT (marked by a vertical dot-dashed line) the ion density falls and a progressive increase in the  $B_x$  and  $B_T$  field components are observed. The increase in field strength represents a build-up of open flux in the magnetotail in response to dayside low latitude magnetopause reconnection occurring with the southward-directed IMF, the substorm “growth phase” (McPherron et al., 1973). The enlargement of the lobe causes the tail magnetopause to flare outwards, such that the impinging solar wind applies a greater normal stress, which must be stood-off by enhanced magnetic pressure in the lobes (e.g. Slavin et al., 2002, and references therein). This enhanced magnetic pressure in the lobes in turn presses inwards on the plasma sheet, which is compressed until the gas pressure reaches equilibrium. This “plasma sheet thinning” or “drop-out” (e.g. Bame et al., 1967; McPherron and Manka, 1985; Fairfield, 1988) results in Cluster returning to the lobe by 01:05 UT, as indicated by the decrease in ion density and  $\beta$  at Cluster.

The increase in lobe field strength thereafter continues, though detailed examination shows that it pauses during the brief northwards turning of the IMF between 01:00 and 01:20 UT, indicating a cessation of dayside reconnection at this time. After continued lobe build-up, a second dipolarization is observed in  $B_z$  at 02:20 UT (second vertical dotted

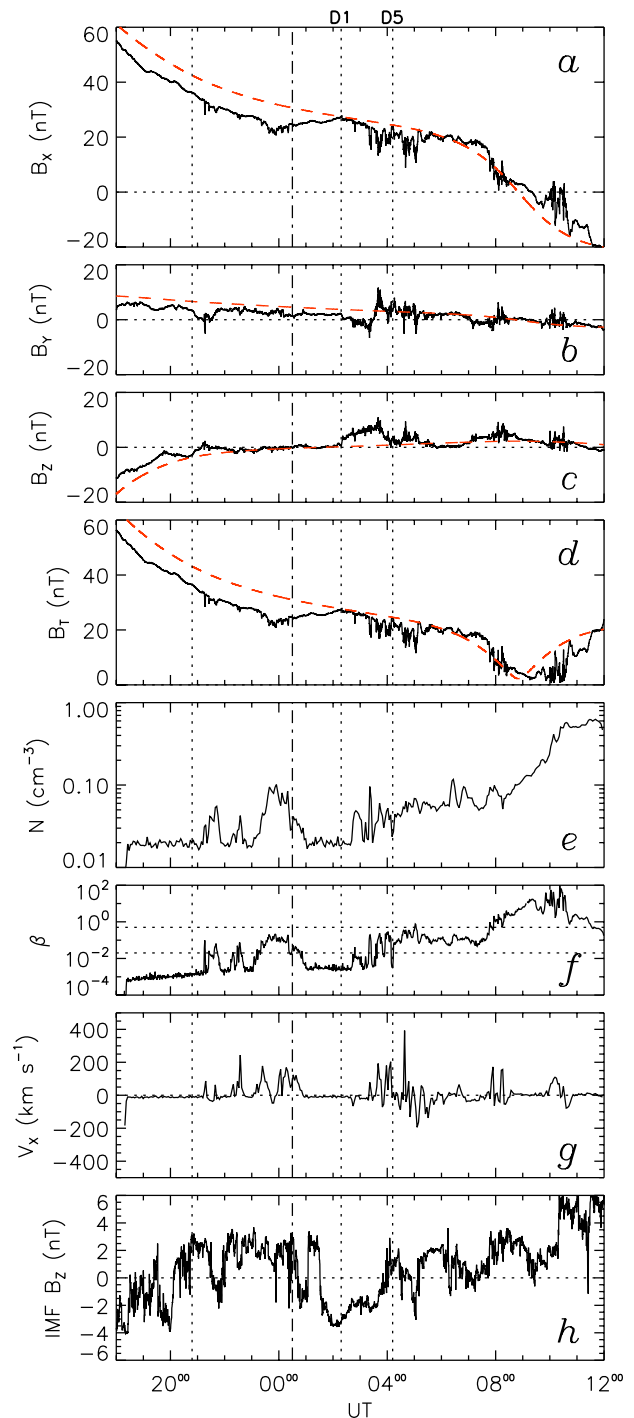


**Fig. 2.** Observations from Cluster-1 for the interval 18:00–12:00 UT, 28–29 August 2004. (a)–(d)  $B_x$ ,  $B_y$ ,  $B_z$ , and  $B_T$  components of the magnetic field in GSM coordinates. Red dashed curves show T96 field predictions. (e) and (f) Ion density and  $V_x$  component of the ion velocity from CIS/HIA. (g) IMF  $B_z$  as measured by ACE, lagged to the magnetopause.

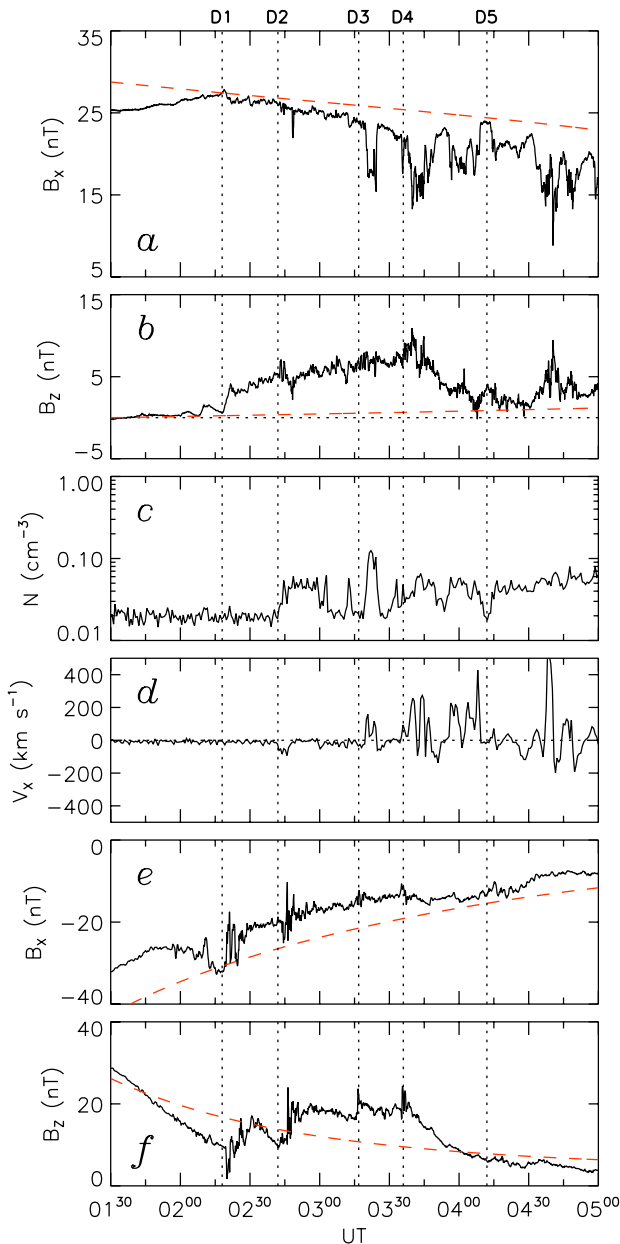


**Fig. 3.** Cluster-1 and Double Star TC1 observations from 01:30–05:00 UT, 29 August 2004. (a) and (b)  $B_x$  and  $B_z$  components of the magnetic field from C1. (c) and (d) Ion density and  $V_x$  ion velocity from C1. (e) and (f)  $B_x$  and  $B_z$  components of the magnetic field from TC1.

line, marked D1), the onset of the second substorm; it is this substorm that forms the focus of the rest of this paper. As with the first substorm, the ion densities at Cluster increase above lobe values approximately 30 min after the dipolarization. Subsequently, a further dipolarization (marked D5) is seen near 04:15 UT.

Eventually, Cluster moves down into the central plasma sheet and crosses the neutral sheet, as indicated by the

increase in the ion density ( $\beta > 0.5$ ) and the transition from a positive to a negative  $B_x$  field component ( $\sim 09:00$  UT).

In what follows, we will concentrate on the observations during the second substorm, first describing the Cluster and Double Star measurements in the near-tail in more detail, and then the associated auroral morphology and ionospheric convection response.

## 2.2 Magnetotail: Cluster and Double Star

We now focus on the time interval leading up to and encompassing the second substorm, 01:30 to 05:00 UT, the interval highlighted on the spacecraft trajectories in Fig. 1. At the start of this interval the Double Star TC1 spacecraft was out-bound through geosynchronous orbit, and reached a down-tail distance of  $X=11 R_E$  by the end, traversing  $4 R_E$  during the three hours. In Fig. 3 we present the  $B_x$  and  $B_z$  components as measured by TC1 for this interval; as before red dotted lines show T96 predictions of the magnetic field. Shown also are the Cluster 1  $B_x$  and  $B_z$  components already shown in Fig. 2, along with  $V_x$  and  $N_i$ . Five vertical lines indicate approximate times of magnetic field dipolarizations which will be described below; these are designated D1–D5, and will be shown in subsequent figures, also. At the start of the interval, Cluster sees an increasing  $B_x$  component, indicating flux build-up in the tail, followed by a dipolarization observed in  $B_z$  at 02:18 UT (D1). At this time,  $N_i$  remains low, indicating that C1 remains in the lobe. However, after 02:42 UT there are episodic enhancements of  $N_i$ , specifically at 02:42, 03:18, and 03:33 UT (these times correspond approximately to D2, D3, and D4). These are associated with transient diamagnetic depressions in  $B_x$  (and the total field magnitude). These indicate that the plasma sheet thickens periodically to engulf the spacecraft. After 03:45 UT the  $B_z$  component of the field gradually decreases, becoming more tail-like and approaching the T96 prediction by 04:00 UT. Finally, we identify a small increase in  $B_z$  near 04:15 UT as D5.

The corresponding TC1 measurements indicate that the spacecraft is located south of the neutral sheet during this period, as  $B_x$  is negative. Increasing (in magnitude)  $B_x$  and decreasing  $B_z$  after 02:00 UT suggest the development of a more tail-like magnetic field configuration during the substorm growth phase, in line with the increasing  $B_x$  seen at C1. At the time of the first dipolarization observed by C1 (D1), TC1 also observes a gradual return of the magnetic field to a more dipolar orientation over 10 min or so. Subsequently, however, sudden dipolarizations are observed at 02:45, 03:16, and 03:36 UT (D2, D3, and D4), corresponding to the entries into the plasmashet of C1. Thereafter,  $B_z$  relaxes to a more tail-like value, approaching the T96 prediction by 04:00 UT, mirroring a similar behaviour observed at C1. In summary, following the initial substorm onset (D1) there are subsequent dipolarizations (D2–D4) observed at TC1 at the same time that further down-tail the plasma sheet thickens to engulf C1.

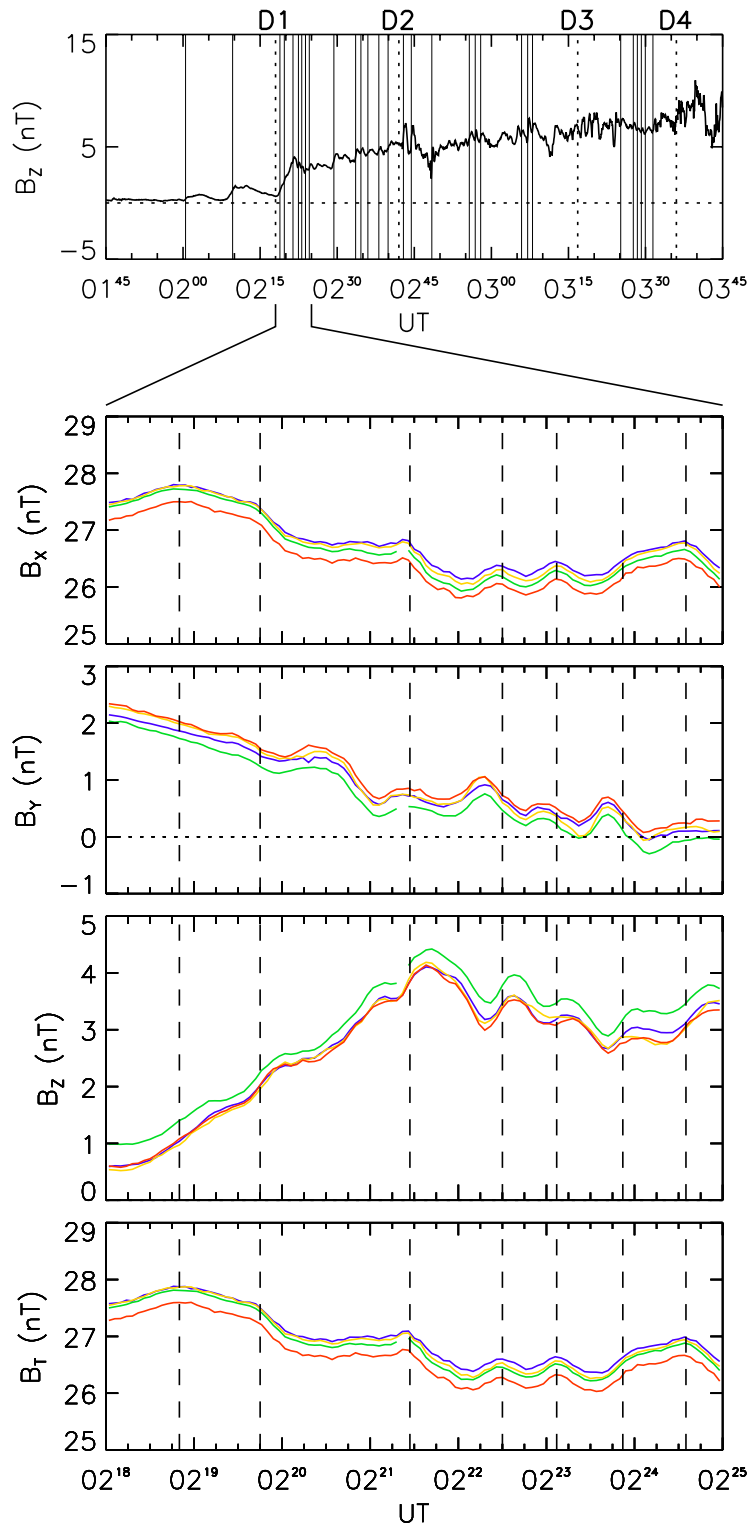


**Fig. 4.** Cluster 1 observations of  $B_z$  from 01:45 to 03:45 UT, showing the occurrence of compression regions associated with plasma sheet flux ropes, together with detailed observations of the event characteristics in  $B_x$ ,  $B_y$ ,  $B_z$ , and  $B_T$  components measured at all four spacecraft between 02:18 and 02:25 UT.

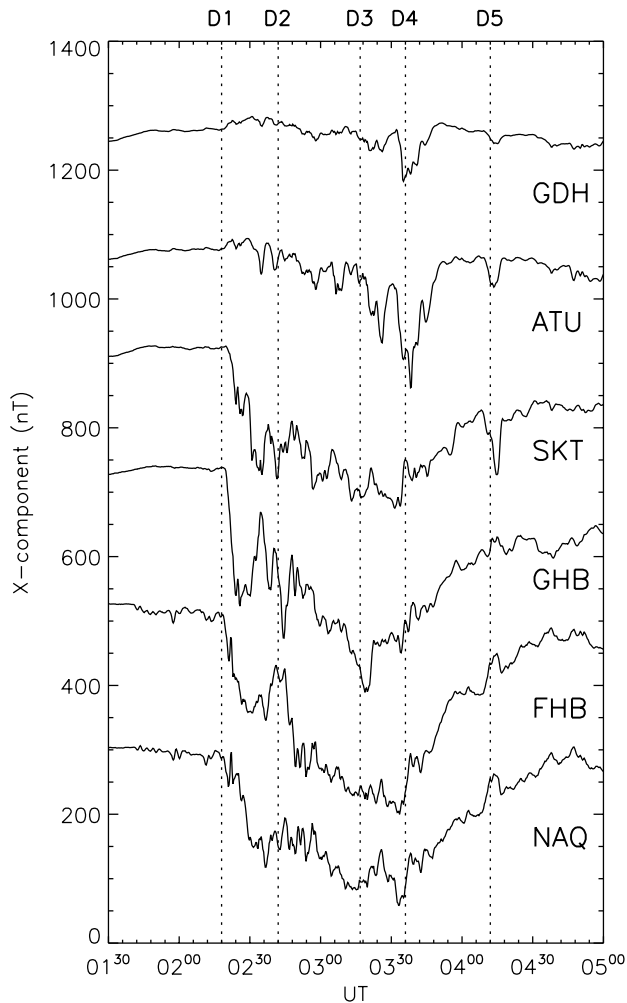


**Fig. 5.** X-component magnetograms from the Greenland West Coast magnetometer chain for the interval 01:30 to 05:00 UT, 29 August 2004.

In addition to these large-scale features, many signatures of small-scale flux ropes in the plasma sheet are seen. The top panel of Fig. 4 shows the  $B_z$  measurements from C1 for the interval 01:45 to 03:45 UT, with D1 to D4 indicated by vertical dotted lines. Marked by thin vertical lines are the times at which flux ropes are identified. The bottom four panels show a blow-up of the period 02:18 to 02:25 UT, with magnetic field measurements from all four Cluster spacecraft. The signatures seen during this period are typical of all the events identified. As described by Slavin et al. (2003, 2005), the plasma sheet flux ropes are identified as compressions of the overlying lobe (in which Cluster is located), that is local enhancements in  $B_x$  and  $B_T$ , known as travelling compression regions (TCRs). Accompanying these are negative-then-positive bipolar excursions of  $B_z$  due to the draping of the field over the plasma sheet bulge; the sense of the excursions is indicative of earthward propagation of

the flux ropes. In  $B_y$  the events are seen as positive-then-negative bipolar signatures. As Cluster is located downwards of the noon-midnight meridian this might indicate that the bulge of the plasma sheet is greatest near the centre of the tail. In all, 30 events are identified, though this will represent only a subset of the total, as these signatures can only be observed when Cluster is located away from the plasma sheet. Slavin et al. (2003, 2005) interpreted multiple observations of flux ropes in the near-tail as an indication of the formation of multiple X-lines. It would appear, then, that multiple X-lines are a feature of the tail throughout the substorm development.

### 2.3 Ionosphere: Greenland magnetometers, IMAGE FUV and SuperDARN

X-component magnetograms from stations of the Greenland West Coast magnetometer chain, which was located in the midnight sector during the interval of interest, are presented in Fig. 5, in order of increasing latitude, spanning the magnetic latitude range 66 to 76°. Each magnetogram is offset by 200 nT for clarity. Vertical lines are shown at the same times as in Fig. 3. The observations show the onset of a ~120 nT negative bay, associated with the development of a westward current, at the four lowest latitude stations at 02:20 UT, the time of the first dipolarization (D1). The negative excursion becomes more pronounced after 02:40 UT (D2), especially at FHB, where the bay eventually exceeds 400 nT in depth. At subsequent dipolarizations, bays appear at ever-higher latitude stations, at ATU after D3 and at ATU and GDH after D4. Further excursions are seen at all stations after the last dipolarization D5, but that at SKT is of greatest amplitude. This last event differs from the previous bays in that the magnetograms suggest a smaller scale current system than before. These observations represent the development and evolution of the substorm current wedge (SCW), the dawn-dusk cross-tail current being diverted through upwards and downwards field aligned currents in the pre- and post-midnight sectors, and closing through a westwards electrojet in the ionosphere (McPherron et al., 1973). The poleward step-wise motion of the magnetogram bays indicates a step-wise development of the SCW, the steps occurring at the times of the dipolarizations observed in the tail.

Auroral observations of the Southern Hemisphere by IMAGE FUV are available from ~01:30 UT onwards, and Fig. 6 shows selected Wideband Imaging Camera (WIC) images from the development of the substorm. Of the two bottom panels, (m) shows a time-series of the maximum brightness observed in the 20-04 MLT sector between magnetic latitudes of 65 and 80°. In addition, we have calculated the magnetic flux threading the dim portion of the ionosphere contained within the auroral oval, presented in panel (n), which we use as a proxy for the open flux in the polar cap,  $F_{PC}$  (e.g. Milan et al., 2003, 2004). We note three caveats associated with this measurement: 1) as will be discussed

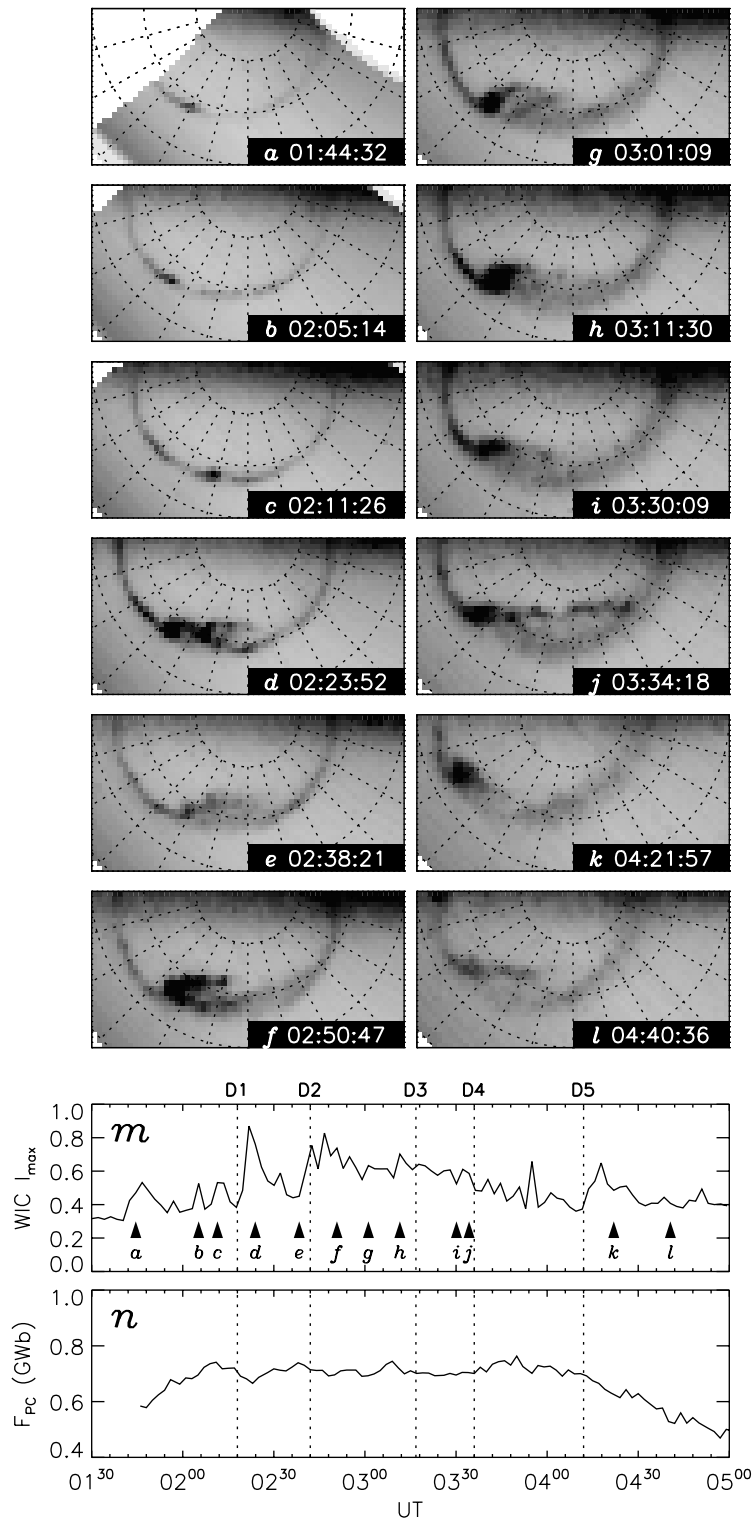


**Fig. 6.** (a)–(l) Selected snapshots of the nightside auroral configuration taken by the FUV/WIC camera onboard IMAGE, presented in a magnetic latitude and local time frame. Latitudes indicated are 60°, 70°, and 80°; local time ranges clockwise from 18:00 MLT, through 00:00 MLT to 06:00 MLT. Darker grey indicates brighter aurora. (m) The maximum auroral brightness (on an arbitrary scale) observed in the local time range 20:00–04:00 MLT and between latitudes of 65° and 80°. (n) An approximate estimate of the open flux content of the magnetosphere  $F_{PC}$ , derived by integrating the magnetic flux through the dim portion of the ionosphere inside the auroral oval.

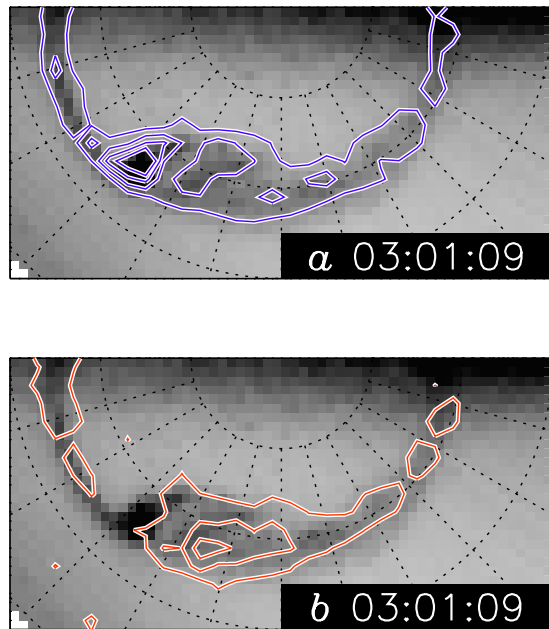


**Fig. 7.** An FUC/WIC auroral snapshot from 03:01 UT (Fig. 6g), superimposed on which are contours of auroral brightness observed by the (a) SI13 and (b) SI12 channels of FUV, sensitive to electrons and protons, respectively.

below, the definition of “dim” is determined by camera sensitivity; 2) the coverage of the WIC camera only allows  $F_{PC}$  to be determined after  $\sim 01:45$  UT; 3) there are certain ambiguities in the pointing information relating to the FUV measurements on this day, and the values of  $F_{PC}$  are subject to some uncertainty. Having said this, these measurements of  $F_{PC}$  are a useful qualitative indicator of the rates of creation and destruction of open flux by reconnection on the dayside and in the magnetotail.

The observations start during the growth phase of the substorm. At this time the auroral oval is dim but is moving to lower latitudes as the polar cap expands,  $F_{PC}$  increasing from 0.6 GWb at 01:45 UT to 0.75 GWb by 02:10 UT. We previously deduced this increase in the open flux content of the magnetosphere during the growth phase from the increase in magnetic field strength at Cluster (Sect. 2.1). Transient, short-lived brightenings of the nightside oval, e.g. panels (a–c) of Fig. 6, are observed prior to the main onset shown in panel (d) at  $\sim 02:20$  UT, associated with D1. This is marked by a considerable brightening of the oval and the development of an auroral bulge. After this time, our deduced value of  $F_{PC}$  remains relatively uniform until 04:00 UT, after which it begins to decrease.

After the initial onset at 02:20 UT, the brightness of the bulge decreases rapidly, so that by 02:38 UT (panel e), it has returned to almost pre-onset levels, though the bulge remains visible. However, the bulge then suddenly re-intensifies at 02:40 UT (D2). Thereafter, the brightness slowly declines

over the next 2.5 h. During this time the auroral bulge shows a slow westwards progression, the main aurora focussed at the westward end to form a westwards-travelling surge (WTS), panels (f–k). During this time there are a few other occasions of note, such as a re-intensification of the whole polewards edge of the auroral bulge at 03:34 UT (D4 and panel j) in what has been described as a poleward boundary intensification (PBI, Lyons et al., 1999), and a re-intensification of the surge head after 04:10 UT (D5 and panel k).

Before moving on, we remark briefly on an interesting observation. The WIC luminosities of Fig. 6 contain contributions from both ion and electron precipitation. Other FUV channels, SI12 and SI13, allow us to discriminate between ions and electrons, respectively. SI12 is sensitive to the Doppler-shifted Lyman  $\alpha$  emissions from down-going hydrogen atoms, that is, precipitating protons which have charge-exchanged during their passage through the atmosphere; there is no contamination from electron aurora. SI13, on the other hand, is sensitive to OI emission at 135.6 nm produced by precipitating electrons, though there may be some small contamination from secondary-electrons produced by precipitating protons. Panels (a–b) of Fig. 7 both reproduce the same WIC snapshot (03:01 UT) from Fig. 6g, typical of the observations from the development and evolution of the WTS. Superimposed on Figs. 7a and b are contours of photon flux observed by SI13 (mainly electrons) and SI12 (ions), respectively. We see that the WTS is associated with a relatively restricted region of electron precipitation, whereas the remainder of the auroral bulge to the east is associated with a more distributed ion precipitation region. We speculate that the ions and electrons represent the charge carriers in the downwards and upwards field-aligned current (FAC) regions associated with the substorm current wedge, described in relation to the Greenland magnetometer signatures of Fig. 5. The upward FAC at the western edge of the bulge has been described before (e.g. Amm et al., 2001), but the location of the closed FAC is still under debate.

Next we present SuperDARN observations of the ionospheric convection flow in the Northern Hemisphere in Fig. 8. Panels (a–d) show four snapshots of the flow in a magnetic latitude and MLT frame, whereas the lower panel presents the time-series of cross-polar cap potential  $\Phi_{PC}$  determined from the convection observations between 01:30 and 05:00 UT. Individual snapshots of the flow are produced by compiling 2-min averages of line-of-sight Doppler velocity observations from 8 Northern Hemisphere radars, which are then used to constrain the solution of an order 6 spherical harmonic expansion of the potential pattern, using the technique of Ruohoniemi and Baker (1998). The vectors indicate the locations of radar observations that contributed to the potential solution; the length and colour of these is related to the flow speed. Where data are sparse, an IMF-driven empirical convection model is usually employed to further constrain the potential pattern. In this study we want to ensure that the

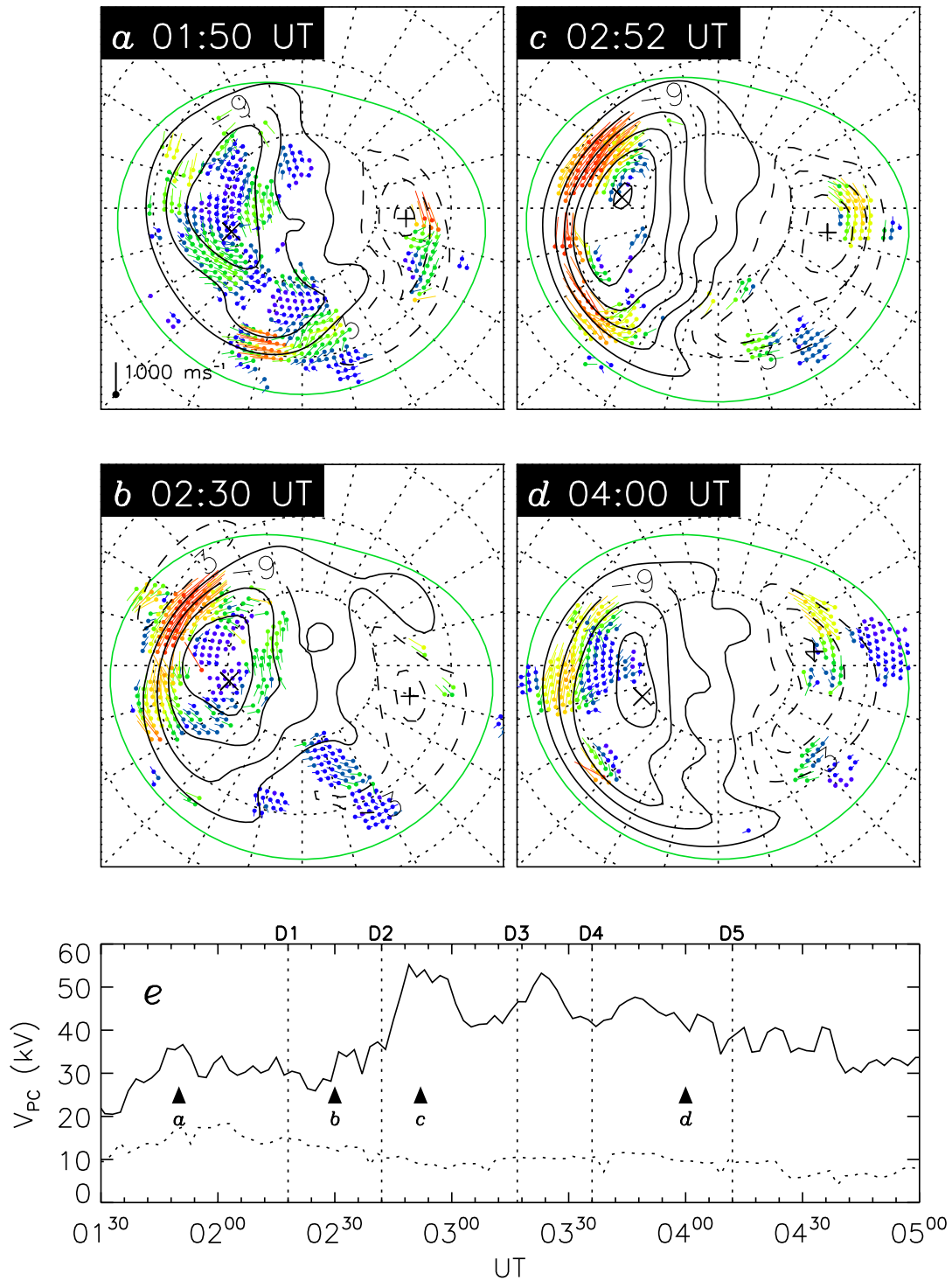


**Fig. 8.** (a)–(d) Selected convection maps derived by the SuperDARN network, shown in a magnetic latitude and MLT frame. Contours of electrostatic potential are separated by intervals of 6 kV. (e) The time series of cross-polar cap potential  $\Phi_{PC}$  derived from the SuperDARN observations (solid curve); the dotted curve gives an indication (on an arbitrary scale) of the number of data points that contribute to each map, showing that there are no sudden appearances or disappearances of regions of backscatter.

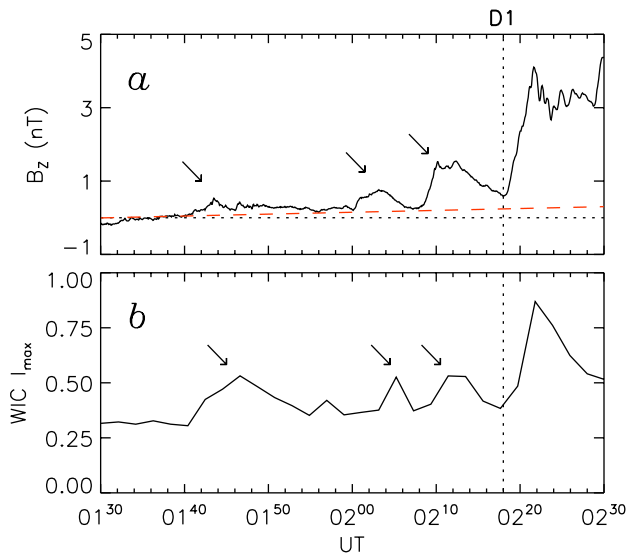


**Fig. 9.** (a)  $B_z$  component of the magnetic field at C1 for the interval 01:30 to 02:30 UT, 29 August 2004. (b) Corresponding auroral brightness from IMAGE FUV/WIC.

model does not overly-contribute to the results, so we employ a “neutral” IMF  $B_x=B_y=B_z=0$  model throughout. Contours show the resulting potential pattern, solid and dashed contours for negative and positive potentials, respectively, with a contour spacing of 6 kV.  $\Phi_{PC}$  is defined as the difference between the minimum and maximum of the potential, the locations of which are indicated by crosses.

As the coverage of the polar region by radar observations is somewhat sparse, the use of the neutral IMF model means that we may underestimate the true value of  $\Phi_{PC}$  somewhat; however, good coverage of the dusk sector return flow means that variations in the strength of the convection pattern will be captured in form, if not in total magnitude. At the start of the interval shown, antisunwards flow across the polar cap and return flow is slow, resulting in  $\Phi_{PC}$  of  $\sim 30$  kV. Around 01:50 UT, panel (a), a small enhancement in flows near midnight gives a small enhancement in  $\Phi_{PC}$ . After 02:00 UT, there is a strengthening of the dusk sector return flow, but this contributes to only a modest increase in  $\Phi_{PC}$ .  $\Phi_{PC}$  rises most dramatically, to  $\sim 50$  kV, after D2, due to a further enhancement of the return flow in both dawn and dusk sectors. Thereafter,  $\Phi_{PC}$  gradually decreases to 30 kV by 05:00 UT, though with enhancements apparent at 03:25 (after D3) and maybe 03:45 UT (after D4). Hence, dipolarizations D2 to D4 are each followed by a  $\sim 15$ -min burst of strengthened convection.

### 3 Discussion

We have presented observations of the development and evolution of an auroral substorm, with Cluster and Double Star

located in the magnetotail, and a variety of ground-based stations measuring convection and current signatures. However, even before substorm onset, interesting small-scale features are observed in the aurora and in the tail, and we describe these first.

#### 3.1 Auroral brightenings (pseudo-breakups) prior to first onset

Prior to substorm onset, during the on-going growth phase, transient dynamic processes are taking place in the tail, which might be classified as pseudo-breakups. Figure 9 focuses on C1 measurements of  $B_z$  and the auroral luminosity observations from 01:30 to 02:30 UT. Three brief and low magnitude dipolarizations (arrows in panel a) can be seen at 01:41, 02:01, and 02:09 UT before the main onset dipolarization (D1) at 02:19 UT. As suggested in Fig. 4, the two events at 02:00 and 02:10 UT can be interpreted as earthward-moving flux ropes. Each of the three events is accompanied by a transient enhancement of the auroral luminosity (arrows in panel b), each also shown in panels (a–c) of Fig. 6. These auroral bursts are relatively localized in nature and each appear at slightly different local times within a 3-h wide MLT sector, though still each produce an observable signature at Cluster. The exact location of the bursts relative to the local time meridian of Cluster is difficult to determine due to uncertainties in the FUV pointing at this time. However, it seems reasonable to suggest that the first two brightenings occur at least 2–3 h of MLT to the west of Cluster. Therefore, although the brightenings are localized in nature in the ionosphere, they produce signatures across a reasonable fraction of the width of the magnetotail. Similar behaviour has previously been reported by Reeves et al. (1990, 1991).

#### 3.2 Substorm development and evolution

To synthesize the observations of the substorm into a coherent picture, we bring together the most salient observations in Fig. 10. Thus, we present again the C1 measurements of (a)  $B_x$ , (b)  $B_z$ , (c)  $N_i$ , and (d)  $V_x$ , and (e) TC1 measurements of  $B_z$ ; panels (f–i) show  $I_{max}$ ,  $F_{PC}$ ,  $\Phi_{PC}$ , and the FHB X-component magnetogram; finally, panel (j) shows IMF  $B_z$ . Vertical lines, as before, indicate the times of dipolarizations. This figure will form the basis of the following discussion. Examination of Fig. 10 allows the substorm development to be described as follows. The initial onset of the substorm as observed in the auroral and magnetometer data is coincident with the first dipolarization seen in  $B_z$  by C1 and TC1 at  $\sim 02:20$  UT (D1). However, even after the initial onset, with its dipolarization and the formation of an auroral bulge, C1 remains in the lobe and there is no enhancement in  $\Phi_{PC}$ .

At the time of the re-intensification at 02:40 UT (D2), the ion density at C1 suddenly increases, indicating an expansion of the plasma sheet northwards over Cluster. This expansion

of the plasma sheet is accompanied by two short positive excursions in  $B_z$ , and ion velocities measured at this time are directed away from the Earth, down the tail, at a speed of  $\sim 75 \text{ km s}^{-1}$ . Shortly afterwards TC1 sees a dipolarization. At the same time,  $\Phi_{PC}$  is observed to increase markedly, and then to remain elevated for the duration of the substorm auroral display. Subsequent dipolarizations at TC1 (D3 and D4) are also each followed by a plasma sheet entry by C1, observed in both  $B_x$  and  $N_i$ , and are also associated with 10–15-min enhancements in  $\Phi_{PC}$ . Although there is no clear response in the aurora at dipolarization D3, dipolarization D4 corresponds to the intensification of the poleward boundary of the auroral bulge (PBI) shown in Fig. 6j.

By 04:00 UT the southward component of the IMF has reduced, and it would appear that the reduction in  $B_z$  observed by both C1 and TC1 occurs in response to this, suggesting that the tail dynamics up until this point have been to some degree driven by continued loading of the lobes with new open flux. Despite the reduction in this driving after 04:00 UT, an auroral re-activation occurs at 04:12 UT in response to a dipolarization observed at C1 (D5), and the reduction in  $F_{PC}$  after this time would suggest that tail reconnection is still ongoing, though  $\Phi_{PC}$  is decreasing in magnitude. After this time, C1 makes further encounters with the plasma sheet. There are no clear signatures observed by TC1 at this time, and so we will not concentrate on this interval in great detail.

### 3.3 Open flux, reconnection rates, and transpolar voltage

Changes in  $F_{PC}$  can be used to infer the dayside and nightside reconnection rates,  $\Phi_D$  and  $\Phi_N$ , respectively, as discussed by Milan et al. (2003, 2006):

$$\frac{dF_{PC}}{dt} = \Phi_D - \Phi_N.$$

The increase in  $F_{PC}$  between 01:45 and 02:10 UT, 0.15 GWb in 25 min, indicates a dayside reconnection rate of  $\sim 100 \text{ kV}$ , assuming that no significant tail reconnection occurs at this time. This corresponds to the interval when the lobe field strength as measured at C1 is also increasing. After D1,  $F_{PC}$  remains constant until  $\sim 04:00$  UT, despite the IMF remaining southward during this period with anticipated continued dayside production of open flux. That is, the closure of magnetic flux by reconnection in the tail must proceed at a rate similar to the addition of open flux to the magnetosphere by reconnection at the dayside. In other words,  $\Phi_D$  and  $\Phi_N$  are roughly equal. This is also consistent with the observations of  $B_x$  by C1 during this period: after D1 the field strength decreases with time, though this decrease is in step with the field prediction of T96 and hence is most likely related to a spatial variation as C1 moves further from the Earth with time, rather than a temporal variation. In other words it would appear that the magnetic pressure in the lobe remains uniform with time, suggesting that the lobe flux content is

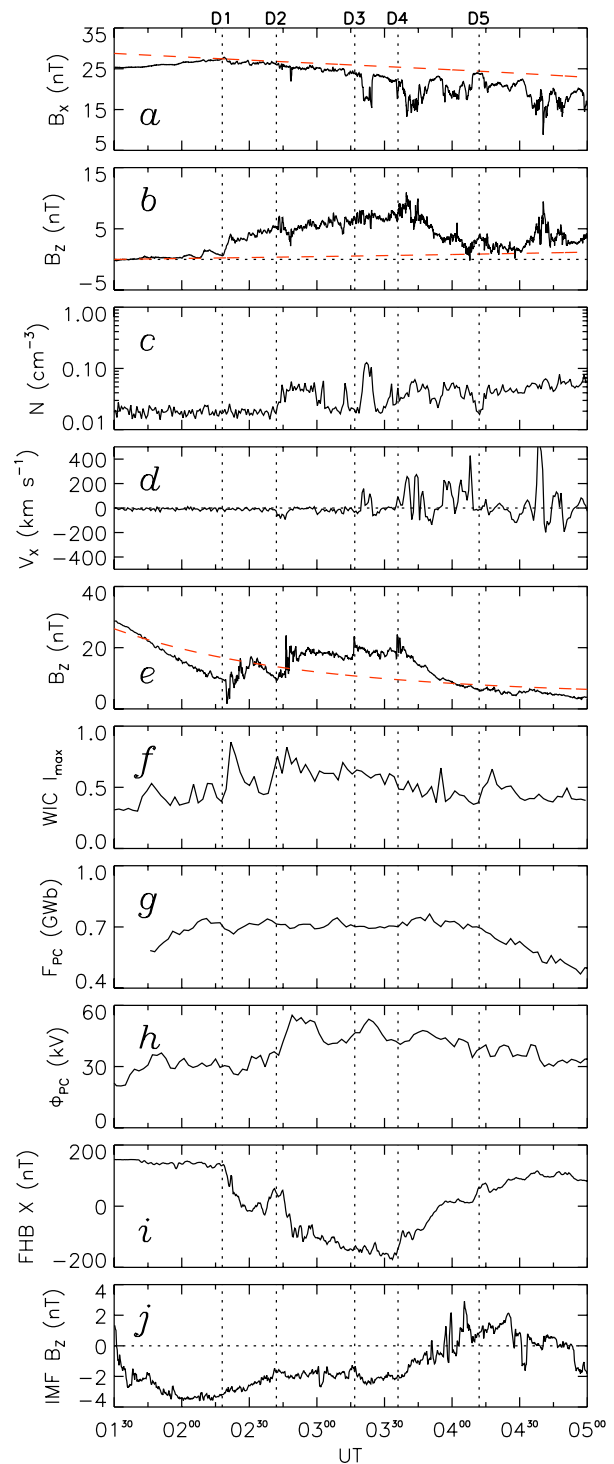


**Fig. 10.** An amalgam of observations from ground and space. (a)  $B_x$  and (b)  $B_z$  from C1. (c) and (d) Ion density and velocity from C1. (e)  $B_z$  from TC1. (f) and (g) Auroral brightness and polar cap flux from IMAGE FUV/WIC. (h) Cross-polar cap potential from SuperDARN. (i) X-component magnetogram from FHB. (j) IMF  $B_z$  from ACE, lagged to the magnetopause.

also constant. We can also show rough consistency between the open flux estimates from the two measurements: if each lobe can be considered as a semi-circle of radius  $20 R_E$  at the down-tail distance of C1, then the lobe field strength of 27 nT as measured at 02:15 UT translates to 0.7 GWb of open flux, close to the value of  $F_{PC}$  calculated at this time.

The rate of flux closure during the substorm is difficult to know exactly; as  $F_{PC}$  remains roughly uniform, then  $\Phi_N \approx \Phi_D$ , but if we wish to quantify  $\Phi_N$  then this requires that we know  $\Phi_D$ . This appears to be  $\sim 100$  kV before substorm onset, but is likely to decrease shortly afterwards as IMF  $B_z$  changes from  $-3.5$  nT to  $-2$  nT. If the reconnection rate is proportional to  $B_z$  (e.g. Milan et al., 2006) then  $\Phi_D$  (and consequently  $\Phi_N$ ) is expected to fall to  $\sim 70$  kV.

As discussed by Milan (2004) and references therein, the transport of open flux across the polar cap, quantified by the cross polar cap potential  $\Phi_{PC}$ , should approximate to the mean of the dayside and nightside reconnection voltages:

$$\Phi_{PC} = \frac{1}{2} (\Phi_D + \Phi_N).$$

In this case, we would expect that  $\Phi_{PC} \approx 50$  kV prior to substorm onset, when  $\Phi_D \approx 100$  kV and  $\Phi_N \approx 0$  kV; after onset, when  $\Phi_D \approx \Phi_N \approx 70$  kV, we expect  $\Phi_{PC} \approx 70$  kV; after the cessation of dayside reconnection once the IMF turned northwards, and assuming that tail reconnection continues unabated at  $\Phi_N \approx 70$  kV, we expect  $\Phi_{PC} \approx 35$  kV. The time-series of  $\Phi_{PC}$  derived from the radar measurements, we concluded above, underestimates the true cross-polar cap potential due to the lack of coverage in the dawn sector. However, the observed variation does reflect the expected changes, varying from 35 kV before onset to 50 kV after onset, to 35 kV after the northward turning of the IMF.

If we speculate that the dipolarizations represent bursts of tail reconnection, then at an average reconnection rate of 70 kV, with a repetition period of  $\sim 30$  min, each burst closes of order 0.125 GWb of flux.

### 3.4 Nightside reconnection of closed or open flux?

Immediately after the development of the main NENL, which we suggest occurs at the first dipolarization D1, reconnection must occur between closed plasma sheet field lines. This process is not thought to occur very efficiently due to the high plasma  $\beta$  of the dense, hot plasma sheet. Due to the relatively low efficiency of this process, the process slows quickly and the attendant auroral signature fades sharply. Newly-reconnected field lines relax Earthwards to increase the density of dipolar-like field lines in the near-Earth tail, leading to the dipolarization observed at TC1 after D1. Tailwards of the X-line newly-reconnected field lines accumulate to begin formation of a plasmoid. However, as no open flux is closed, there is little rearrangement of the flux in the tail, so no significant convection is excited. However, the reconnection does remove closed field lines from the vicinity of

the neutral line relieving the build-up of pressure in the lobe (and hence  $B_x$  at C1 stops increasing at D1).

If this is the case, then the initial formation of the auroral bulge and poleward motion of the luminosity after D1 must occur on closed field lines, though we have until now assumed that all the dim portion poleward of the pre-substorm oval was open. In other words, there is a region of dim, closed field lines poleward of the main pre-onset auroral oval. We assume, then, that these closed field lines stretch a long distance down-tail and do not contain much plasma. Sub-visual precipitation on closed field lines poleward of the main nightside auroral luminosity have previously been reported by Mende et al. (2003), and the possible existence of such a region was suggested as an uncertainty in measuring  $F_{PC}$  from auroral observations by Milan et al. (2003). In the present case, then, our estimate of  $F_{PC}$  prior to substorm onset will have been an overestimate, by slightly less than 0.1 GWb (the flux contained within the bulge that develops between D1 and D2). This will be discussed further in Sect. 3.7.

We conclude, then, that the second dipolarization (D2) represents the transition from reconnection of closed field lines to the reconnection of open field lines. This occurs in tandem with an increase in  $\Phi_{PC}$ , enhanced and prolonged auroral luminosities, and, we expect, the release of a plasmoid. Figure 11 focuses on the FGM observations from all four Cluster spacecraft for the period surrounding D2. At 02:42:30 UT, C1, C2, and C4 observe a  $\sim 1$  nT enhancement in  $B_T$  lasting  $\sim 45$  s; a similar signature at C3 lasts only  $\sim 15$  s. After 02:44:15 UT, all four spacecraft observe another enhancement in  $B_T$ , though with a brief dip in the centre of the event. Both events also involve a  $\sim 2$  nT increase in  $B_z$  and a similar decrease in  $B_y$ . We interpret these as the signatures of plasmoid release, observed as travelling compression regions (TCRs) in the lobe (e.g. Slavin et al., 2002, 2003); these events are considerably larger than the small flux rope signatures examined in Fig. 4. The increase in total field strength is associated with a bulge in the plasma sheet compressing the overlying lobe field lines, and the re-orientation of  $B_y$  and  $B_z$  is due to draping over the bulge. Careful comparison of CIS/HIA densities and temperatures from C1 and C3 for this interval reveals that in association with the first event C3 briefly entered the PSBL, in association with the early decrease in  $B_T$ . During the second event, both entered the PSBL, again during the dip in  $B_T$ . This suggests that during the first plasmoid event C1, C2, and C4 observed the TCR in the lobe, whereas C3, located nearest the equatorial plane (see inset in Fig. 1 for the tetrahedral configuration at this time), entered the high density plasmoid itself. In the second event, all four spacecraft saw the field enhancement in the lobe, and then all four entered the plasmoid at the time of passage of the thickest point of the bulge. Finally, after 02:48 UT, there is a 4-nT reduction in  $B_T$  of 1-min duration observed by all four spacecraft. We interpret this as the passage of a third plasmoid by which all spacecraft

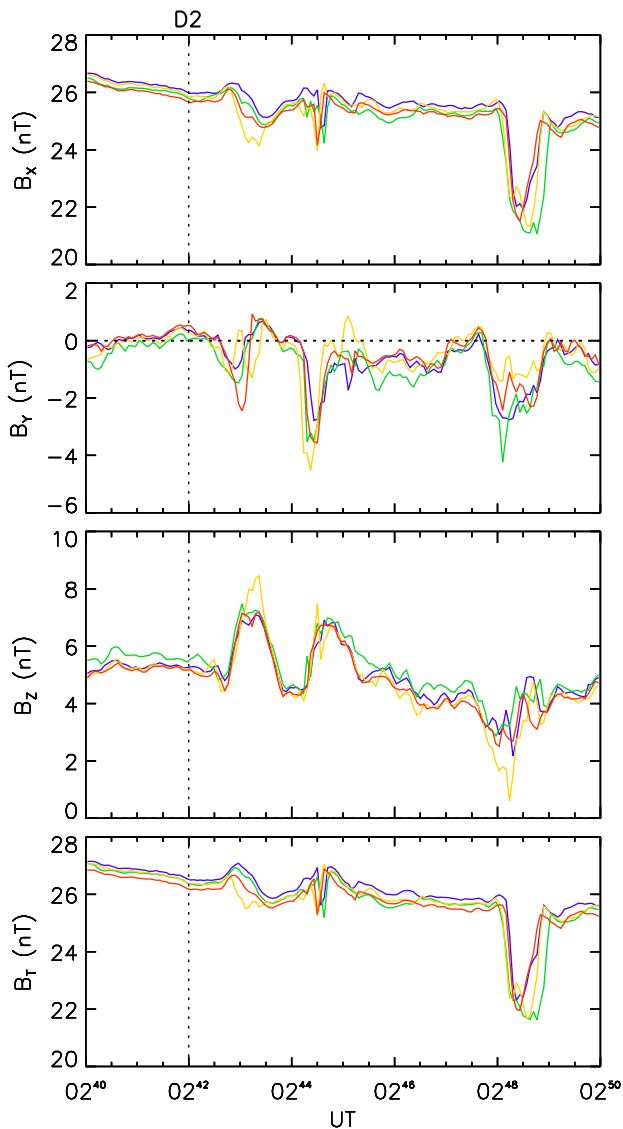


**Fig. 11.** Magnetic field components  $B_x$ ,  $B_y$ ,  $B_z$ , and  $B_T$  from all four Cluster spacecraft (blue, green, yellow, red are C1–C4, respectively), for the interval 02:40 to 02:50 UT, 29 August 2004.

are engulfed, or at least a transient thickening of the plasma sheet. The nested nature of the four traces during this event suggests that the bulge advances from below and duskwards of the Cluster constellation, and subsequently retreats back in the same direction. This may suggest that the bulge is thickest near the noon-midnight meridian of the tail.

### 3.5 Location of X-line

The observation of several plasmoids in the 5 min or so following D2, together with the presence of many flux ropes preceding and following this, suggests that by this time multiple X-lines have formed in the near-tail, consistent with previous interpretations (e.g. Slavin et al., 2003, 2005).

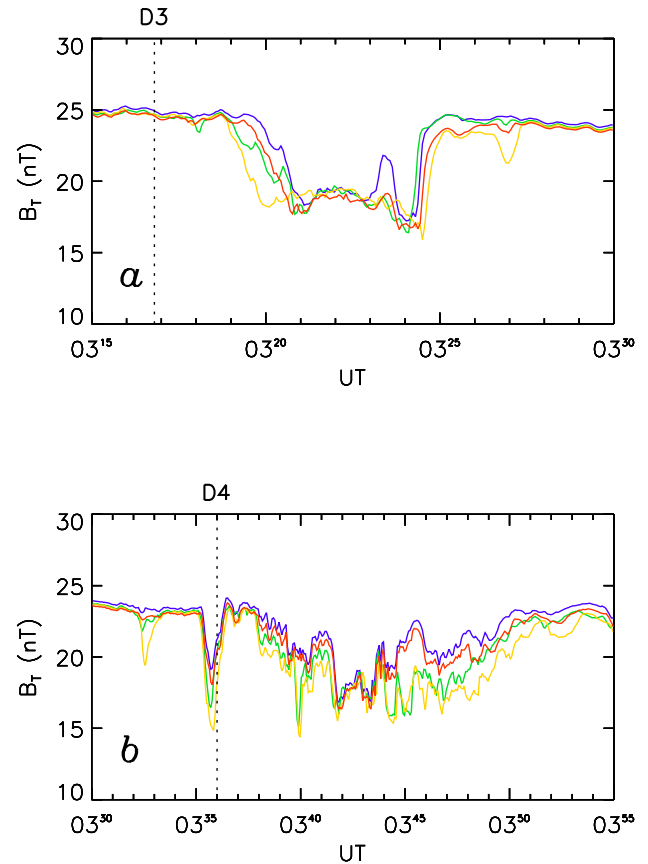


**Fig. 12.** Total magnetic field strength  $B_T$  from all four Cluster spacecraft for the intervals (a) 03:15 to 03:30 UT, and (b) 03:30 to 03:55 UT, 29 August 2004.

Unfortunately, the four-spacecraft FGM observations do not allow a very straightforward determination of the direction of propagation, tailwards or Earthwards, of the plasmoids described in Sect. 3.4. However, the small-scale flux ropes appear consistently to move earthwards, suggesting that the main active X-line is tailward of Cluster. On the other hand, the ion moments in the PSBL encounters around the time of D2 indicate tailward plasma motion, which would seem to suggest that the X-line is located earthward of the tetrahedron. Due to the inconsistency of these signatures, we hesitate to draw a firm conclusion as to the location of the X-line around the time of D2.

Later dipolarizations, especially D3 and D4, are followed by deeper entries of Cluster into the plasma sheet, as evidenced by the higher densities and deeper reductions in  $B_x$  observed for longer periods of time. This may be in part due to its approach of the equatorial plane as Cluster continues in its orbit, which appears to reduce the sensitivity to multiple plasmoid features as seen following D2. However, the characteristics of the plasma sheet encounter of D3 and D4 are investigated in Figs. 12a and b, respectively. D3 is nested in a similar manner to the third event following D2, but the details

of the entrance to and exit from the plasma sheet by the four spacecraft suggest that the bulge grows from below and then propagates towards dawn. Ion moments reveal earthwards streaming plasma at the crossings of the PSBL as Cluster enters and exits the bulge. We are confident that the active X-line is now tailward of Cluster.

The plasma sheet encounter after D4 is different again (Fig. 12b), having a less nested appearance and indicating that C2 and C3 enter deeper into the plasma sheet than C1 and C4. This again suggests that the bulge is thickest near the noon-midnight meridian. Ion velocities are again directed earthwards during this encounter, indicating that reconnection occurs tailward of Cluster.

We expect the location of the main tail X-line to progress down-tail with time, as previously suggested by Hones (1979). Indeed, the motion of the X-line has been suggested to jump in a step-wise fashion, a new X-line forming in the neutral sheet each time further down-tail than the previous X-line. This is accompanied by poleward steps in the SCW current system observed by the ground magnetometers at each dipolarization, indicating new open flux is closed at each step. It is interesting to note that following the sudden dipolarization of the field at Cluster at D1, the field continues to become more dipolar with time,  $B_z$  further increasing and  $B_x$  further decreasing with respect to the T96 predictions, until about 03:45 UT when the IMF turns northwards (Figs. 10a and b). The same is true of the field at TC1 (Fig. 10e). We interpret this as continued and increasing magnetic flux pile-up in the tail near TC1 and Cluster following substorm onset. This pile-up should be relieved by the convection of closed field lines from the nightside to the dayside, and indeed the transpolar voltage is elevated throughout this period. However, the convection is clearly not sufficiently rapid to remove flux from the pile-up region as quickly as it is added by reconnection at the X-line, which itself is continuously being supplied by new open flux due to on-going dayside reconnection. This sluggish convection may be a consequence of elevated ionospheric conductance in the region of the auroral bulge, and the associated frictional coupling with the neutral atmosphere. For this reason the auroral bulge expands polewards and the SCW steps polewards. It was suggested by Baumjohann (2002) that it is the pile-up of closed flux in the near-tail, and the expansion tailwards of this pile-up region, that forces the tail X-line to migrate down-tail.

We can estimate the down-tail motion of the X-line by considering the amount of flux closed following each dipolarization ( $\sim 0.1$  GWb, Sect. 3.3) and the  $B_z$  component of the magnetic field crossing the neutral sheet within the pile-up region. If the latter is estimated to be 10 nT, the approximate average of the C1 and TC1  $B_z$  measurements during the flux build-up period (Fig. 3), then each burst of reconnection closes flux that occupies a cross-sectional area of  $10^{16}$  m<sup>2</sup> through the neutral sheet. If this is distributed across the width of the magnetotail, approximately  $40 R_E$ , then it extends a distance of  $6 R_E$  down-tail; if it occupies

only a fraction of the width of the tail, then it extends correspondingly further. If no convection of this newly-closed flux towards the dayside occurred, then this would be the approximate distance that the X-line would be pushed between each dipolarization. Assuming that the down-tail motion of the X-line was continuous, and did not occur in steps, then averaging over the duration between dipolarizations, the X-line has a velocity of  $\sim 20$  km s<sup>-1</sup>. With non-zero but sluggish convection, this becomes an overestimate, but provides a qualitative explanation for the motion of the X-line.

Following the cessation of dayside reconnection after 03:45 UT the pile-up region decays, the field returning to a more tail-like configuration at TC1 and Cluster. This implies that the pile-up can now be convected away faster than closed flux is produced by tail reconnection, though reconnection does continue as indicated by the contraction of the polar cap and elevated auroral activity after D5. We suggest, then, that the tail reconnection rates subsides significantly after 03:45 UT, as the dayside reconnection rate relaxes, only to increase again at D5 with the formation of a new tail X-line. This would explain the appearance of the D5 SCW magnetic bay near SKT, equatorward of that associated with D4: by this time convection has relieved the pile-up region and re-distributed flux within the polar cap and auroral zone such that the open/closed field line boundary in the ionosphere has relaxed to lower latitude.

It is interesting to note that subsequent to D5, the first significant build-up of dipolar field lines near Cluster, as seen by the increase in  $B_z$  at C1, occurs after 04:30 UT (Fig. 10b). A similar signature is seen at TC1 (Fig. 10e), though now the increase in  $B_z$  is smaller than during the earlier pile-up as TC1 is further down-tail than previously. This occurs shortly after a brief return to southward IMF: it is possible again that new open flux transported into the tail is once again influencing the tail dynamics.

### 3.6 Substorm triggers

This study interval contains what we consider to be 2 main substorm onsets (20:45 UT and 02:19 UT). We have studied in detail the second substorm, comprising an initial onset and four subsequent re-intensifications, each marked by a dipolarization. It is interesting to note that the first substorm onset occurred during an interval of northward IMF (Fig. 2), whereas the second substorm and its first 3 re-intensifications occurred during southward IMF; the last intensification of the second substorm occurred during northward IMF. As discussed in Sect. 2.1, it is possible to think of substorm onset as the magnetospheric response to increasing pressure in the neutral sheet, caused by the accumulation of open flux in the magnetotail lobes during the growth phase and the associated flaring of the tail magnetopause. In this case, it is to be expected that expansion phase onset will generally occur during periods of southward IMF. While this is true for D1–D4, it is

not true for D5 or the first substorm. These, then, appear to contradict the simple picture presented above.

However, we note now that the onset of the first substorm coincides with a step-like enhancement in the solar wind dynamic pressure (not shown) from 0.63 to 0.8 nPa, a 25% increase. Thus, even without an increase in the tail flare, the pressure exerted on the magnetopause and hence the neutral sheet will be increased. This may be sufficient to trigger onset.

In the case of D5, no similar enhancement in solar wind pressure is seen. However, even after the preceding tail reconnection associated with D1 to D4, the polar cap has not contracted (Fig. 10g), as open flux has been continuously added at the dayside. So, even though the IMF is now directed northwards, similar conditions still exist in the tail that pertained at the original substorm onset. For this reason, the tail may still be unstable and desire to reduce the open flux content of the lobes, thereby reducing the tail cross-section and easing pressure on the neutral sheet.

### 3.7 Summary of reconnection rates

We summarize the preceding discussion of the reconnection rates and changes in open flux during the substorm in Fig. 13. Panel (a) shows schematically the variation in the open flux  $F_{PC}$  (full line) through the course of the substorm. Panel (b) represents the reconnection rates. The dashed line shows the dayside reconnection rate,  $\Phi_D$ , the rate of creation of open flux. This is initially high as the IMF is directed southwards, and only subsides after the northward-turning of the IMF after D4. Initially, then,  $F_{PC}$  is growing: the substorm growth phase. After the onset of the substorm at D1 the NENL is reconnecting closed flux, and we represent this as  $\Phi_{NC}$ , the nightside closed flux reconnection rate, represented by the dotted curve in Fig. 13b. Open flux is still created at the dayside at this time, so  $F_{PC}$  continues to grow. However, our estimates of the open flux content of the magnetosphere have been based on the size of the dim region within the auroral oval, which we have now argued contains  $\sim 0.1$  GWb of dim closed flux (Sect. 3.4); in other words, we have overestimated the quantity of open flux. We represent this in Fig. 13a as the dotted line labelled  $F_{PC}+F_{DC}$ , where  $F_{DC}$  is the size of the dim closed flux region. As this closed flux is reconnected by the NENL and brightens to form the initial auroral bulge,  $F_{DC}$  decreases, and  $F_{PC}+F_{DC}$  approaches  $F_{PC}$ ; by D2 our estimates of the open flux content become increasingly accurate.

After D2, open flux is closed at the NENL, represented by the full line in Fig. 13b,  $\Phi_{NO}$  being the nightside reconnection rate of open flux.  $\Phi_{NO}$  must be close to  $\Phi_D$  as  $F_{PC}$  is observed to become uniform with time. There will be variations in  $\Phi_{NO}$  in response to the step-wise motion of the NENL at D3 and D4, but overall  $\Phi_{NO}$  appears to track  $\Phi_D$ , to the extent that that as  $\Phi_D$  subsides at the northward-turning of the IMF  $\Phi_{NO}$  decreases also, such that

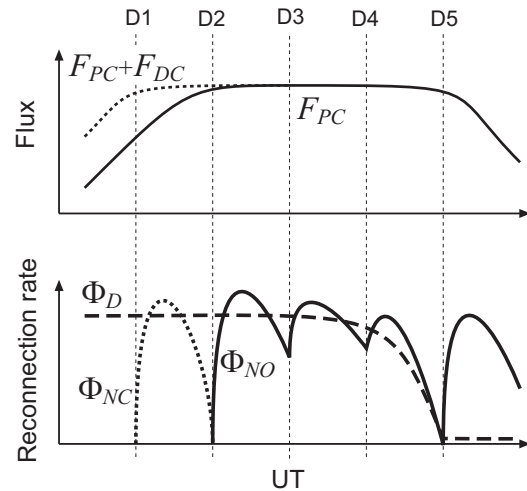


**Fig. 13.** A schematic representation of the open and dim-closed magnetic flux inside the auroral oval, and day- and nightside reconnection rates during the substorm (see text for details).

$F_{PC}$  remains constant through-out this period. However, the magnetotail is still stressed and reconnection finally commences once again, accompanied by the fifth dipolarization D5, to further close open flux. At this time  $\Phi_{NO}$  dominates over  $\Phi_D$  and  $F_{PC}$  decreases.

## 4 Conclusions

We summarize the main findings of this paper as follows:

- 1) The substorm starting at 02:19 UT on 29 August 2004 has a two-stage onset, which we interpret as the reconnection of closed field lines by a near-Earth neutral line (NENL) prior to the explosive onset of reconnection of open flux. The first stage is associated with the short-lived development of a small auroral bulge, and the observation of a modest convection bay in ground magnetometers. The second stage is associated with prolonged nightside auroral activity and the formation of a westward-travelling surge, a large convection bay, the excitation of significant ionospheric convection, and plasmoid release. Throughout the substorm period, compression regions in the lobe suggest the presence of many small-scale, earthward-travelling flux ropes in the plasma sheet.
- 2) There is a region of subvisual aurora on closed field lines polewards of the quiescent nightside auroral oval. This may occupy up to 0.1 GWb of flux. This closed flux has to be reconnected prior to plasmoid release and the reconnection of open lobe field lines. The size of this region indicates the amount of flux contained in the plasmoid. As suggested by Milan et al. (2003), this subvisual closed flux region has to be accounted for when

determining the open flux content of the magnetosphere from auroral observations during geomagnetically quiet periods. Following substorm onset, however, this region becomes aurorally active, and the ambiguity in the relationship between the poleward boundary of the nightside auroral oval and the open/closed field line boundary (OCB) is removed.

- 3) Following the onset of open flux closure, repeated dipolarizations are observed in the tail, separated by 20–30 min. We interpret these as step-wise movements of the NENL down-tail in response to flux pile-up in the near-tail. Each step tailwards is associated with the formation of a new substorm current wedge at ever-higher latitudes, and a step-wise poleward motion of convection bays observed at the ground. Each dipolarization is also accompanied by an enhancement in the cross-polar cap potential. Approximately 0.1 GWb of open flux is reconnected between each dipolarization.
- 4) Flux pile-up is controlled by the competition between the rates of reconnection at the NENL and convection of newly-closed flux away from the nightside. The former appears to be closely controlled by the dayside reconnection rate, which, if active re-supplies the lobes with new open flux to maintain pressure on the neutral sheet. The latter will be controlled by frictional coupling between ionosphere and neutral atmosphere in the auroral bulge region. After onset the IMF remains directed southwards and the pile-up region grows. Correspondingly the NENL must move down-tail, away from the pile-up region. Simple calculations indicate that X-line motion should occur at a speed approaching  $20 \text{ km s}^{-1}$  down-tail. It is only after a northward-turning of the IMF that the pile-up region begins to subside, as convection now dominates. Hence, the dynamics of the tail during the substorm seem to be strongly-driven by the on-going level of solar wind-magnetosphere coupling at the dayside.
- 5) After the pile-up region subsides, due to the northward-turning of the IMF, there is a further dipolarization. We suggest that this is because the tail is still in a highly-stressed state, despite the preceding 2 h of substorm activity. That is, we estimate that by this time  $\sim 0.3 \text{ GWb}$  of open flux have been closed by the NENL, but an equivalent amount of flux have been opened at the dayside during the same period. Further tail activity is required to close sufficient lobe flux to allow the magnetotail to relax to a less flared configuration and relieve pressure on the plasma sheet.

*Acknowledgements.* This study was conducted under the auspices of the Cluster and Double Star Ground-Based Working Group (CDSGBWG). Cluster analysis at Imperial College is supported by PPARC. E. Lucek is supported by a PPARC fellowship. We

would like to thank N. F. Ness of the Bartol Research Institute and D. J. McComas of the Southwest Research Institute for the provision of data from ACE MFI and ACE SWEPAM, respectively.

Topical Editor T. Pulkkinen thanks a referee for her/his help in evaluating this paper.

## References

- Amm, O., Janhunen, P., Kauristie, K., Opgenoorth, H. J., Pulkkinen, T. I., and Viljanen, A.: Mesoscale ionospheric electrodynamics observed with the MIRACLE network: 1. Analysis of a pseudo-breakup spiral, *J. Geophys. Res.*, 106, 24 675–24 690, 2001.
- Balogh, A., Dunlop, M. W., Cowley, S. W. H., Southwood, D. J., Thomlinson, J. G., Glassmeier, K.-H., Musmann, G., Lühr, H., Buchert, S., Acuña, M. H., Fairfield, D. H., Slavin, J. A., Riedler, W., Schwingenschuh, K., and Kivelson, M. G.: The Cluster magnetic fields investigation, *Space Sci. Rev.*, 79, 65–91, 1997.
- Balogh, A., Carr, C. M., Acuña, M. H., Dunlop, M. W., Beek, T. J., Brown, P., Fornaçon, K.-H., Georgescu, E., Glassmeier, K.-H., Harris, J., Musmann, G., Oddy, T., and Schwingenschuh, K.: The Cluster Magnetic Field Investigation: overview of in-flight performance and initial results, *Ann. Geophys.*, 19, 1207–1217, 2001.
- Bame, S. J., Ashbridge, J. R., Felthaus, H. E., Hones, E. W., and Strongly, I. B.: Characteristics of the plasma sheet in the Earth's magnetotail, *J. Geophys. Res.*, 72, 113–129, 1967.
- Baumjohann, W.: Modes of convection in the magnetotail, *Phys. Plasmas*, 9, 3665–3667, 2002.
- Borälöv, E., Opgenoorth, H. J., Kauristie, K., Lester, M., Bosqued, J. M., Dewhurst, J. P., Owen, C. J., Dunlop, M., Slavin, J. A., Fazakerley, A., and Perry, C.: Correlation between ground-based observations of substorm signatures and magnetotail dynamics, *Ann. Geophys.*, 23, 997–1011, 2005.
- Cowley, S. W. H. and Lockwood, M.: Excitation and decay of solar wind-driven flows in the magnetosphere-ionosphere system, *Ann. Geophys.*, 10, 103–115, 1992.
- Dungey, J. W.: Interplanetary magnetic fields and the auroral zones, *Phys. Rev. Letters*, 6, 47–48, 1961.
- Escoubet, C. P., Fehringer, M., and Goldstein, M. L.: The Cluster mission – Introduction, *Ann. Geophys.*, 19, 1197–1200, 2001.
- Escoubet, C. P., Schmidt, R., Goldstein, M. L., Cluster – Science and mission overview, *Space Sci. Rev.*, 79, 11–32, 1997.
- Fairfield, D. H.: Multi-point measurements of magnetotail dynamics, *Adv. Space Res.*, 8, 97–108, 1988.
- Fairfield, D. H. and Ness, N. F.: Configuration of the geomagnetic tail during substorms, *J. Geophys. Res.*, 75, 7032–7047, 1970.
- Greenwald, R. A., Baker, K. B., Dudeney, J. R., Pinnock, M., Jones, T. B., Thomas, E. C., Villain, J.-P., Cerisier, J.-C., Senior, C., Hanuise, C., Hunsucker, R. D., Sofko, G., Koehler, J., Nielsen, E., Pellinen, R., Walker, A. D. M., Sato, N., and Yamagishi, H.: DARN/SuperDARN: A global view of the dynamics of high-latitude convection, *Space Sci. Rev.*, 71, 761–796, 1995.
- Heppner, J. P.: Recent measurements of the magnetic field in the outer magnetosphere and boundary regions, *Space Sci. Rev.*, 7, 166–190, 1967.
- Hones Jr., E. W.: Transient phenomena in the magnetotail and their relation to substorms, *Space Sci. Rev.*, 23, 393–410, 1979.
- Lockwood, M. and Cowley, S. W. H.: Ionospheric convection and the substorm cycle, in *Proceedings of the International Confer-*

- ence on Substorms (ICS-1), 99–109, 1992.
- Lyons, L. R., Nagai, T., Blanchard, G. T., Sason, J. C., Yamamoto, T., Mukai, T., Nishida, A., and Kokubun, S.: Association between Geotail plasma flows and auroral poleward boundary intensifications observed by CANOPUS photometers, *J. Geophys. Res.*, 104, 4485–4500, 1999.
- McComas, D. J., Bame, S. J., Barker, P., Feldman, W. C., Phillips, J. L., Riley, P., and Griffée, J. W.: Solar Wind Electron Proton Alpha Monitor (SWEPAM) for the Advanced Composition Explorer, *Space Sci. Rev.*, 86, 563–612, 1998.
- McPherron, R. L. and Manka, R. H.: Dynamics of the 1054 UT, March 22, 1979 substorm, *J. Geophys. Res.*, 90, 1175–1190, 1985.
- McPherron, R. L., Russell, C. T., and Aubry, M. P.: Satellite studies of magnetospheric substorms on August 15, 1968, 9, Phenomenological model for substorms, *J. Geophys. Res.*, 78, 3131–3149, 1973.
- Mende, S. B., Heeterks, H., Frey, H. U., Lampton, M., Geller, S. P., Habraken, S., Renotte, E., Jamar, C., Rochus, P., Spann, J., Fuselier, S. A., Gerard, J.-C., Gladstone, R., Murphree, S., and Cogger, L.: Far ultraviolet imaging from the IMAGE spacecraft, 1. System design, *Space Sci. Rev.*, 91, 243–270, 2000a.
- Mende, S. B., Heeterks, H., Frey, H. U., Lampton, M., Geller, S. P., Abiad, R., Siegmund, O. H. W., Tremsin, A. S., Spann, J., Dougani, H., Fuselier, S. A., Magoncelli, A. L., Bumala, M. B., Murphree, S., and Trondsen, T.: Far ultraviolet imaging from the IMAGE spacecraft, 2. Wideband FUV imaging, *Space Sci. Rev.*, 91, 271–285, 2000b.
- Mende, S. B., Carlson, C. W., Frey, H. U., Peticolas, L. M., and Ostgaard, N.: FAST and IMAGE-FUV observations of a substorm onset, *J. Geophys. Res.*, 108, doi:10.1029/2002JA009787, 2003.
- Milan, S. E.: Dayside and nightside contributions to the cross polar cap potential: placing an upper limit on a viscous-like interaction, *Ann. Geophys.*, 22, 3771–3777, 2004.
- Milan, S. E., Cowley, S. W. H., Lester, M., Wright, D. M., Slavin, J. A., Fillingim, M., Carlson, C. W., and Singer, H. J.: Response of the magnetotail to changes in open flux content of the magnetosphere, *J. Geophys. Res.*, 109, A04220, doi:10.1029/2003JA010350, 2004.
- Milan, S. E., Wild, J. A., Grocott, A., and Draper, N. C.: Space and ground-based investigations of solar wind-magnetosphere-ionosphere coupling, *Adv. Space Res.*, in press, 2006.
- Milan, S. E., Lester, M., Cowley, S. W. H., Oksavik, K., Brittnacher, M., Greenwald, R. A., Sofko, G., and Villain, J.-P.: Variations in polar cap area during two substorm cycles, *Ann. Geophys.*, 21, 1121–1140, 2003.
- Popov, V. A., Papitashvili, V. O., and Watermann, J. F.: Modelling of equivalent ionospheric currents from meridian magnetometer chain data, *Earth Planets Space*, 53, 129–137, 2001.
- Reeves, G. D., Fritz, T. A., Cayton, T. E., and Belian, R. D.: Multisatellite measurements of the substorm injection region, *Geophys. Res. Lett.*, 17, 2015–2018, 1990.
- Reeves, G. D., Belian, R. D., and Fritz, T. A.: Numerical tracing of energetic particle drifts in a model magnetosphere, *J. Geophys. Res.*, 96, 13997–14008, 1991.
- Rème, H., Bosqued, J.-M., Sauvaud, J. A., Cros, A., Dandouras, I., Aoustin, C., Bouyssou, J., Camus, Th., Cuvilo, J., Martz, C., M'Edale, J. L., Perrier, H., Romefort, D., Rouzaud, J., d'Uston, C., Möbius, E., Crocker, K., Granoff, M., Kistler, L. M., Popecki, M., Hovestadt, D., Klecker, B., Paschmann, G., Scholer, M., Carlson, C. W., Curtis, D. W., Lin, R. P., McFadden, J. P., Formisano, V., Amata, E., Bavassano-Cattaneo, M.-B., Baldetti, P., Belluci, G., Bruno, R., Chionchio, G., Di Lellis, A., Shelley, E. G., Ghielmetti, A. G., Lennartsson, W., Korth, A., Rosenbauer, H., Lundin, R., Olsen, S., Parks, G. K., McCarthy, M., and Balsiger, H.: The Cluster Ion Spectrometry (CIS) Experiment, *Space Sci. Rev.*, 79, 303–350, 1997.
- Rème, H., Aoustin, C., Bosqued, J.-M., Dandouras, I., Lavraud, B., Sauvaud, J. A., Barthe, A., Bouyssou, J., Camus, Th., Coeur-Joly, O., Cros, A., Cuvilo, J., Ducay, F., Garbarowitz, Y., Medale, J. L., Penou, E., Perrier, H., Romefort, D., Rouzaud, J., Vallat, C., Alcayde, D., Jacquey, C., Mazelle, C., d'Uston, C., Möbius, E., Kistler, L. M., Crocker, K., Granoff, M., Moukikis, C., Popecki, M., Vosbury, M., Klecker, B., Hovestadt, D., Kucharek, H., Kuenneth, E., Paschmann, G., Scholer, M., Sckopke, N., Seidenschwang, E., Carlson, C. W., Curtis, D. W., Ingraham, C., Lin, R. P., McFadden, J. P., Parks, G. K., Phan, T., Formisano, V., Amata, E., Bavassano-Cattaneo, M. B., Baldetti, P., Bruno, R., Chionchio, G., Di Lellis, A., Marcucci, M. F., Pallochia, G., Korth, A., Daly, P. W., Graeve, B., Rosenbauer, H., Vasyliunas, V., McCarthy, M., Wilber, M., Eliasson, L., Lundin, R., Olsen, S., Shelley, E. G., Fuselier, S., Ghielmetti, A. G., Lennartsson, W., Escoubet, C. P., Balsiger, H., Friedel, R., Cao, J.-B., Kovrazhkin, R. A., Papamastorakis, I., Pellat, R., Scudder, J., and Sonnerup, B.: First multispacecraft ion measurements in and near the Earth's magnetosphere with the identical Cluster ion spectrometry (CIS) experiment, *Ann. Geophys.*, 19, 1303–1354, 2001.
- Ruohoniemi, J. M. and Baker, K. B.: Large-scale imaging of high-latitude convection with Super Dual Auroral Radar Network HF radar observations, *J. Geophys. Res.*, 103, 20 797–20 811, 1998.
- Slavin, J. A., Fairfield, D. H., Lepping, R. P., Hesse, M., Ieda, A., Tanskanen, E., Østgaard, N., Mukai, T., Nagai, T., Singer, H. J., and Sutcliffe, P. R.: Simultaneous observations of earthward flow bursts and plasmoid ejection during magnetospheric substorms, *J. Geophys. Res.*, 107, doi:10.1029/2000JA003501, 2002.
- Slavin, J. A., Owen, C. J., Dunlop, M. W., Borälv, E., Moldwin, M. B., Sibeck, D. G., Tanskanen, E., Goldstein, M. L., Fazakerley, A., Balogh, A., Lucek, E., Richter, I., Rème, H., and Bosqued, J. M.: Cluster four spacecraft measurements of small travelling compression regions in the near-tail, *Geophys. Res. Lett.*, 30, doi:10.1029/2003GL018438, 2003.
- Slavin, J. A., Tanskanen, E. I., Hesse, M., Owen, C. J., Dunlop, M. W., Imber, S., Lucek, E. A., Balogh, A., and Glassmeier, K.-H.: Cluster observations of traveling compression regions in the near-tail, *J. Geophys. Res.*, 110, doi:10.1029/2004JA010878, 2005.
- Smith, C. W., Acuña, M. H., Burlaga, L. F., L'Heureux, J., Ness, N. F., and Scheifele, J.: The ACE Magnetic Fields Experiment, *Space Sci. Rev.*, 86, 613–632, 1998.
- Stone, E. C., Frandsen, A. M., Mewaldt, R. A., Christian, E. R., Marglies, D., Ormes, J. F., and Snow, F.: The Advanced Composition Explorer, *Space Sci. Rev.*, 86, 1–22, 1998.
- Tsyganenko, N. A. and Stern, D. P.: Modelling the global magnetic field of the large-scale Birkeland current systems, *J. Geophys. Res.*, 101, 27 187–27 198, 1996.